

Detailed analysis of the poorly studied northern open cluster NGC 1348 using multi-color photometry and GAIA EDR3 astrometry.

D. Bisht^{1*}, Qingfeng Zhu¹, W. H. Elsanhoury^{2,3}, Devesh P. Sariya⁴, Geeta Rangwal⁵, R. K. S. Yadav⁶, Alok Durgapal⁵, Ing-Guey Jiang⁴

¹Key Laboratory for Researches in Galaxies and Cosmology, University of Science and Technology of China, Chinese Academy of Sciences, Hefei, Anhui, 230026, China

²Astronomy Department, National Research Institute of Astronomy and Geophysics (NRIAG), 11421, Helwan, Cairo, Egypt (Affiliation ID: 60030681)

³Physics Department, Faculty of Science and Arts, Northern Border University, Turaif Branch, Saudi Arabia

⁴Department of Physics and Institute of Astronomy, National Tsing Hua University, Hsin-Chu, Taiwan.

⁵Center of Advanced Study, Department of Physics, D. S. B. Campus, Kumaun University Nainital 263002, India.

⁶Aryabhata Research Institute of Observational Sciences, Manora Peak, Nainital 263002, India.

*E-mail: dbisht@ustc.edu.cn

Received ; Accepted

Abstract

The membership determination for open clusters in noisy environments of the Milky Way is still an open problem. In this paper, our main aim is provide the membership probability of stars using proper motions and parallax values of stars using Gaia EDR3 astrometry. Apart from the Gaia astrometry, we have also used other photometric data sets like UKIDSS, WISE, APASS and Pan-STARRS1 in order to understand cluster properties from optical to mid-infrared regions. We selected 438 likely members with membership probability higher

than 50% and $G \leq 20$ mag. We obtained the mean value of proper motion as $\mu_x = 1.27 \pm 0.001$ and $\mu_y = -0.73 \pm 0.002$ mas yr⁻¹. The cluster's radius is determined as 7.5 arcmin (5.67 pc) using radial density profile. Our analysis suggests that NGC 1348 is located at a distance of 2.6 ± 0.05 kpc. The mass function slope is found to be 1.30 ± 0.18 in the mass range 1.0–4.1 M_\odot , which is in fair agreement with Salpeter's value within the 1σ uncertainty. The present study validates that NGC 1348 is a dynamically relaxed cluster. We computed the apex coordinates (A, D) for NGC 1348 as $(A_\odot, D_\odot) = (-23^\circ.815 \pm 0^\circ.135, -22^\circ.228 \pm 0^\circ.105)$. In addition, calculations of the velocity ellipsoid parameters (VEPs), matrix elements μ_{ij} , direction cosines (l_j, m_j, n_j) and the Galactic longitude of the vertex have been also conducted in this analysis.

Key words: open clusters and associations: individual (NGC 1348) — Astrometry— Dynamics— Kinematics

1 Introduction

Open clusters (OCs) have been used to find out the spiral arm structure and evolution of the Galactic disk (Trumpler 1930, Janes & Adler 1982, Carraro et al. 1998, Chen et al. 2003, Piskunov et al. 2006, Moraux 2016). Due to their location in the disc, open clusters are highly contaminated by the non-member stars. Data from the Gaia mission is very helpful in this direction. In continuation of its previous two data releases the (early) Third data release (hereafter EDR3; Gaia Collaboration et al. 2020) was made public on 3rd December 2020. This catalog consists of the central coordinates, proper motions in right ascension and declination and parallaxes $(\alpha, \delta, \mu_\alpha \cos \delta, \mu_\delta, \pi)$ for more than 1.46 billion sources. Gaia EDR3 has enabled a breakthrough in OC studies because it provides accurate information of proper motion and parallaxes for a large number of stars. Cantat-Gaudin et al. (2018) reported membership probabilities for 1229 OCs with 60 previously unknown clusters based on the Gaia data. One of the most important outcome from the Gaia data is that we can detect many new OCs. Sim et al. (2019), Liu & Pang (2019) and Castro-Ginard et al. (2020) identified 207, 76 and 582 new OCs in the Galactic disk. In this paper, our main goal is to perform a detailed analysis of NGC 1348 using Gaia data. The open cluster NGC 1348 ($\alpha_{2000} = 03^h 34^m 06^s$, $\delta_{2000} = 51^\circ 24' 30''$; $l=146^\circ.969$, $b=-3^\circ.709$) is located in the second Galactic quadrant. Carraro (2002) analyzed this object using CCD UBVI data. He found that NGC 1348 is a significantly reddened cluster ($E(B - V) = 0.85$), lies at a distance 1.9 ± 0.5 kpc and has an age greater than 50 Myr.

Open clusters contain a spectrum of stellar masses (from very low to high mass stars) formed

from the same molecular cloud. This makes them the ideal objects to study the initial mass function (IMF). Many authors have studied IMF in open clusters (Durgapal & Pandey 2001, Phelps & Janes 1993, Piatti et al. 2002, Piskunov et al. 2004, Scalo et al. 1998, Sung and Bessell 2004, Yadav & Sagar 2002, 2004, and Bisht et al. 2017 & 2019). The universality of IMF is still a matter of intense debate (Elmegreen 2000; Larson 1999; Marks et al. 2012; Dib 2014; Dib, Schmeja & Hony 2017). One of the motives of the present analysis is to gather information of the IMF to understand the star formation history in NGC 1348. The mass segregation studies in the OCs provide information about the distribution of stars according to their masses within the cluster region. The information contained in both the mass distribution of stars and their spatial distribution can help us understand the process of star formation. We also investigate the orbits of stars in NGC 1348 as these are very useful to constrain the role of external tidal forces and help us better understand the dynamical evolution of the cluster.

Virtually, members of a star cluster appear as coherent and mutually associated moving groups of stars sharing similar properties like distance, kinematics, chemical composition, and age as well as the line of sight velocity (radial velocity). The determination of the convergent point coordinates (A_\odot, D_\odot) at which the stars of the cluster seem to be merging (i.e. apex) is an important parameter in the kinematical and physical examination (Wayman 1965, Hanson 1975, Eggen 1984, Gunn et al. 1988). To determine the apex, numerous techniques are available in the literature, like i) classical convergent point method, ii) the AD-chart method, and iii) convergent point search method (CPSM; Galli et al. 2012). The convergent point method is a classical method which still attracts the interest of many working groups. This method allows selecting stars based on the parallelism of the proper motion components. It was further developed and discussed by Smart (1938), Brown (1950), & Jones (1971). Based on the works by Jones (1971) and de Bruijne (1999), Galli et al. (2012) presented the CPSM which also uses the proper motion data. The CPSM represents the stellar proper motions by great circles over the celestial sphere and visualizes their intersections as the convergent point of the moving group. However, for a complete picture of a star's space motion, both proper motions and radial velocities are required. Thus, one can identify the stellar groupings with a common movement in space via the AD-chart method based. This method that takes into account the individual stellar apexes is discussed by Chupina et al. (2001, 2006). In this work, we adopted the AD-chart method (stellar apex method) for NGC 1348. We used the distribution of individual apexes of cluster members in the equatorial coordinate system. Also, some kinematical parameters and velocity ellipsoid parameters (VEPs) are presented here with the computational algorithm presented in our previous papers (Elsanhoury et al. 2015, 2018, Postnikova et al. 2020, Bisht et al. 2020).

The structure of the article is as follows. A brief description of the different data sets used here

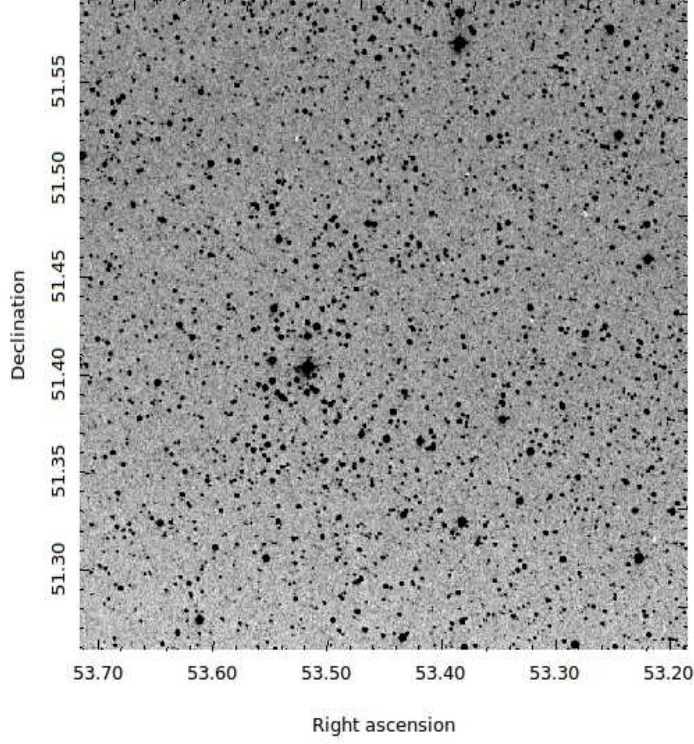


Fig. 1. The identification map of NGC 1348 taken from the DSS.

is given in Section 2. In Section 3, we performed the study of proper motion and selected the cluster member stars. The structural properties the cluster and derivation of its fundamental parameters are explained in Section 4. Section 5 deals with the study of Luminosity and mass function while the mass segregation is described in Section 6 along with dynamical and kinematical analysis of the cluster. We conclude the present work in Section 7.

2 Data

We extracted photometric data of the cluster within a 10 arcmin radius from the APASS, Pan-STARRS1, UKIDSS and WISE along with astrometric data from GAIA EDR3. The main purpose is to take different photometric surveys' data to check the extinction law towards the open cluster NGC 1348 from the optical to the mid-infrared. After cross-matching all these catalogs, the fundamental parameters, mass function, Galactic orbits and kinematics have been studied in the current paper. The identification map shown in the Fig. 1 is taken from the Digitized Sky Survey (DSS). The descriptions

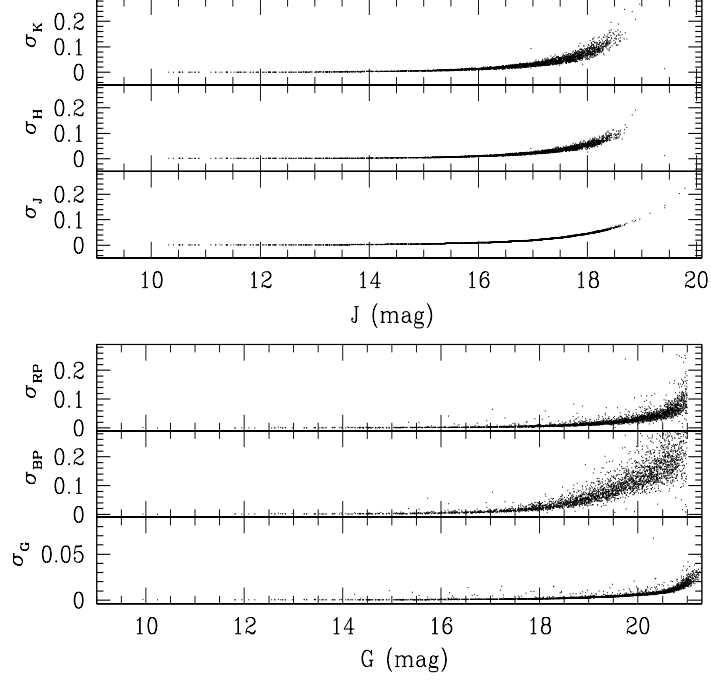


Fig. 2. Photometric errors in the J , H and K magnitudes against J magnitude (upper panels). Photometric errors in the Gaia pass bands G , G_{BP} and G_{RP} against G magnitude (lower panels).

of the above mentioned data sets are as following:

2.1 GAIA EDR3

We have used GAIA EDR3 (Gaia Collaboration et al. 2020) data for the astrometric investigation of NGC 1348. This data consists of five quantities, which are position coordinates, parallaxes and proper motions in two directions having a limiting magnitude of $G = 21$ mag. We have plotted the errors in the three photometric bands (G , G_{BP} and G_{RP}) along with their G magnitudes as shown in the three bottom panels of Fig 2. For the sources having $G \leq 15$ mag, the uncertainties in parallax are ~ 0.02 - 0.03 mas while for the sources with $G \leq 17$ mag, it is ~ 0.07 . In Fig. 3, we plotted the proper motion and their corresponding errors as a function of G magnitude. This figure shows that the maximum error in proper motion components is ~ 0.4 mas/yr upto $G \sim 20$ mag.

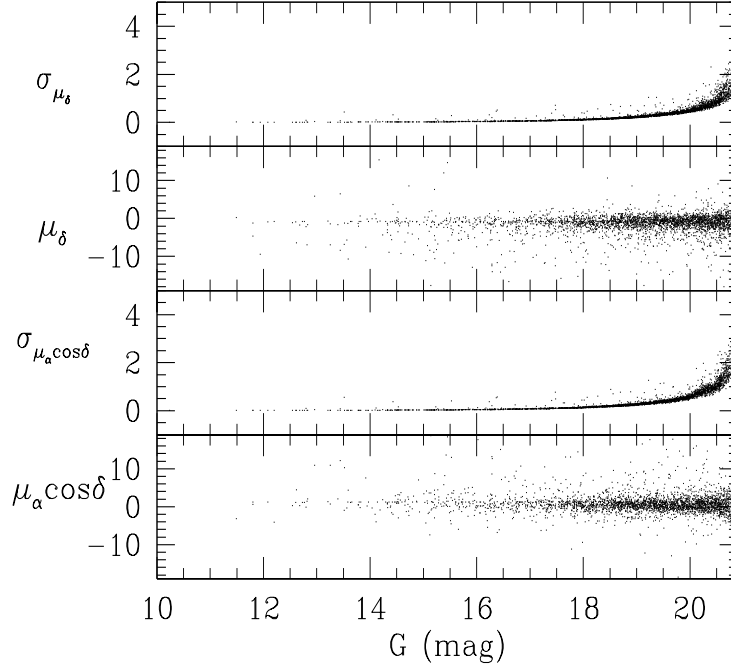


Fig. 3. Plot of Proper motions and their errors versus G magnitude. The unit of proper motions and their errors is mas/yr.

2.2 UKIDSS

The UKIRT Infrared Deep Sky Survey (UKIDSS; Lawrence et al. 2007) is a deep large scale infrared survey organized with the Wide Field Camera (WFCAM; Casali et al. 2007) on UKIRT. The UKIDSS GCS DR9 covers ~ 36 square degrees observed in five passbands (Z, Y, J, H, K ; Hewett et al. 2006).

2.3 WISE

The WISE database contains photometric magnitudes of stars in the mid-IR bands. The effective wavelength of these bands are $3.35\mu m(W1)$, $4.60\mu m(W2)$, $11.56\mu m(W3)$ and $22.09\mu m(W4)$ (Wright et al. 2010). We have extracted data from the ALLWISE source catalog for NGC 1348.

2.4 APASS

The American Association of Variable Star Observers (AAVSO) Photometric All-Sky Survey (APASS) is cataloged in five filters: B, V (Landolt) and g', r', i' , with V band magnitude range

from 7 to 17 mag (Heden & Munari 2014). The DR9 catalog covers about 99% of the sky (Heden et al. 2016). From here, we have used data in B and V bands for NGC 1348.

2.5 Pan-STARRS1

The Pan-STARRS1 survey (Hodapp et al. 2004) provides data in five broad-band filters, g , r , i , z , y , screening from 400 nm to 1 μm (Stubbs et al. 2010). These data have a mean 5- σ point source limiting sensitivities as 23.3, 23.2, 23.1, 22.3, and 21.4 mag in g , r , i , z , and y bands respectively (Chambers et al. 2016). The filters have an effective wavelengths of 481, 617, 752, 866, and 962 nm, respectively (Schlafly et al. 2012; Tonry et al. 2012).

3 Mean Proper motion and Membership probability of stars

We plotted a diagram between the Proper motions (PMs) ($\mu_\alpha \cos \delta$, μ_δ) which is called Vector Point Diagrams (VPDs) and shown in the bottom panels of Fig. 4. The top and middle panels shows that the corresponding G versus ($G_{BP} - G_{RP}$) and J versus ($J - H$) color magnitude diagrams (CMDs). The left panel shows all stars within a radius of 10 arcmin around the cluster center, while the middle and right panels show the probable cluster members having similar motion in the sky and non-member stars, respectively. The selection of circle's radius as 0.6 mas/yr in VPD is a compromise between losing stars with poor PMs and the contamination of field stars. The CMD of the selected probable cluster members is shown in the upper-middle panels in Fig. 4. The main sequence of the cluster is clearly separated from the non members.

For the mean proper motion estimation, we consider the only probable cluster members on the basis of clusters VPD and CMD as shown in Fig. 4. By using weighted mean method, we found the mean-proper motion of NGC 1348 as 1.27 ± 0.001 and -0.73 ± 0.002 mas yr $^{-1}$ in RA and DEC directions, respectively.

In this paper, we used the method described by Balaguer-Núñez et al. (1998) by using Gaia EDR3 catalog data for NGC 1348 to estimate the membership probability of stars. This method has been used for several clusters by various authors (Yadav et al. 2013; Sariya et al. 2021a, 2021b; Bisht et al. 2020). Recently we have adopted the above membership probability method for few OCs using Gaia EDR3 data (Bisht et al. 2021a, Bisht et al. 2021b). We used stars with PM errors ≤ 0.5 mas/yr to express cluster and field star distributions. A group of stars is found at $\mu_{xc}=1.27$ mas yr $^{-1}$, $\mu_{yc}=-0.73$ mas/yr. Considering a distance of 2.6 kpc and radial velocity dispersion of 1 km s $^{-1}$ for open star clusters (Girard et al. 1989), the expected dispersion (σ_c) in PMs would be 0.08 mas/yr. For the non-members, we obtained $(\mu_{xf}, \mu_{yf}) = (-1.0, -1.7)$ mas/yr and $(\sigma_{xf}, \sigma_{yf}) = (3.9, 2.6)$ mas/yr.

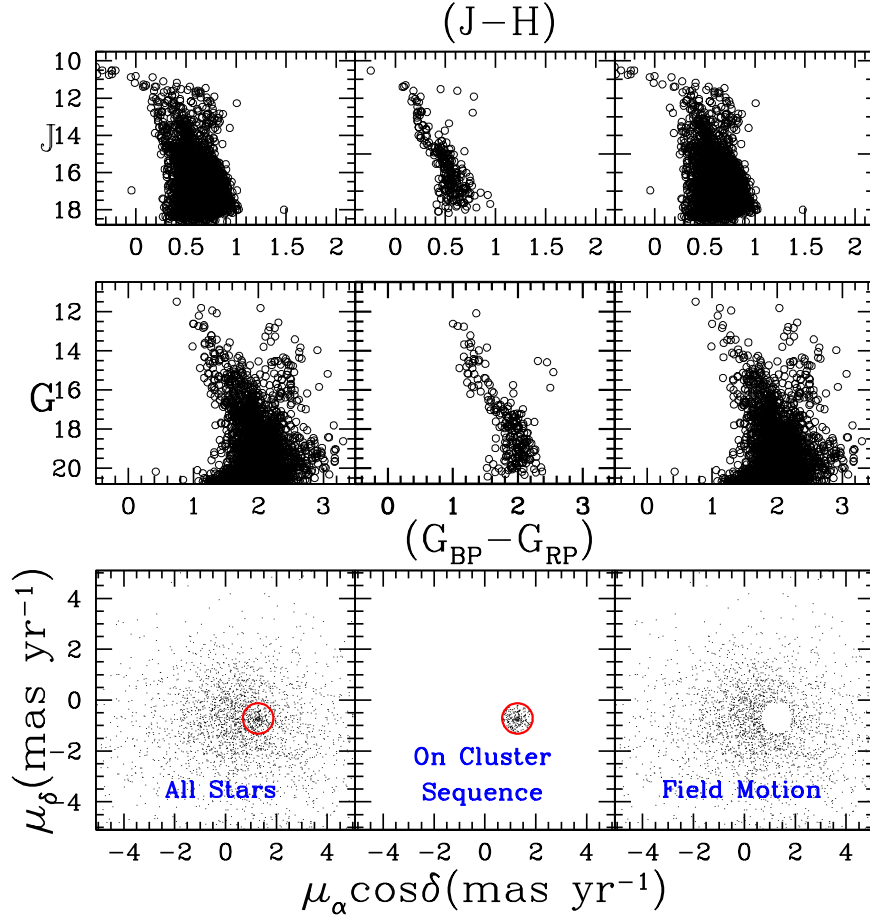


Fig. 4. (Bottom panels) Proper-motion vector point diagrams (VPDs) for NGC 1348. (Top panels) J versus $(J - H)$ color magnitude diagrams. (Middle panels) G versus $(G_{BP} - G_{RP})$ color magnitude diagrams. (Left panel) The entire sample. (Center) Stars within the circle of 0.6 mas yr^{-1} radius centered around the mean proper motion. (Right) Probable background/foreground field stars in the direction of the cluster. All these plots show only the stars with PM error smaller than 0.5 mas yr^{-1} in each coordinate.

Based on the above method, 438 stars are selected as member stars with membership probability higher than 50% and $G \leq 20$ mag. In the left panel of Fig. 5, we plotted membership probability versus G magnitude. In this figure, we can see a clear separation of the cluster and the field stars. In the right panel of this figure, we plotted G magnitude versus parallax of stars. The most probable cluster members with high membership probability ($\geq 50\%$) are shown by red dots in Fig. 5. we have plotted G versus $(G_{BP} - G_{RP})$ CMD, the identification chart and proper motion distribution using stars with membership probability higher than 50% in Fig. 6. The Cantat-Gaudin et al. (2018) catalog reports membership probabilities for the stars of this cluster but only up to 18 mag in G band. Here, We provide the most probable cluster members up to 20 mag in G band which is fainter than Cantat-Gaudin et al. (2018).

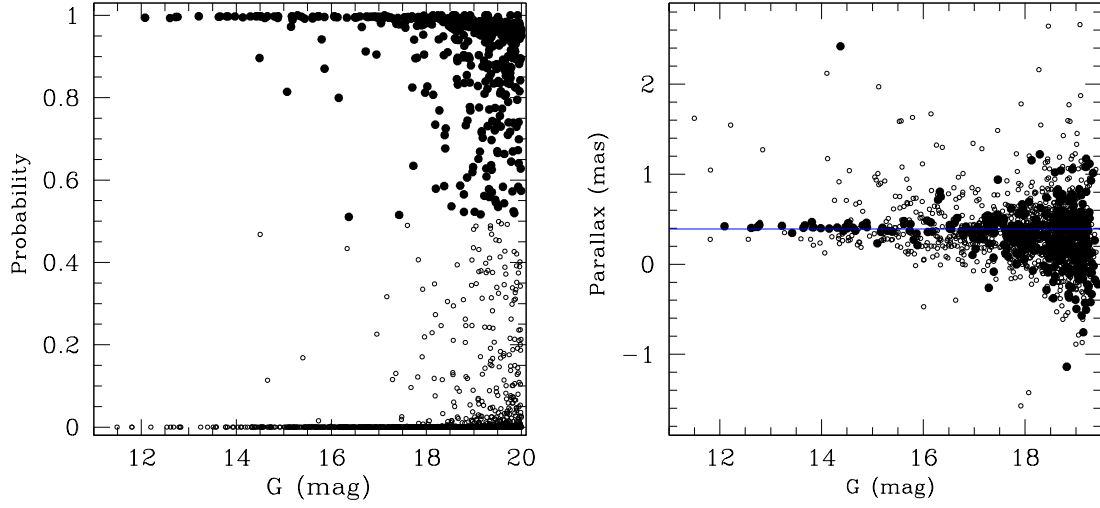


Fig. 5. (Left panel) The cluster membership probabilities plotted with G magnitude. (Right panel) Cluster parallax with G magnitude. Solid black dots are probable cluster members with membership probability higher than 50%.

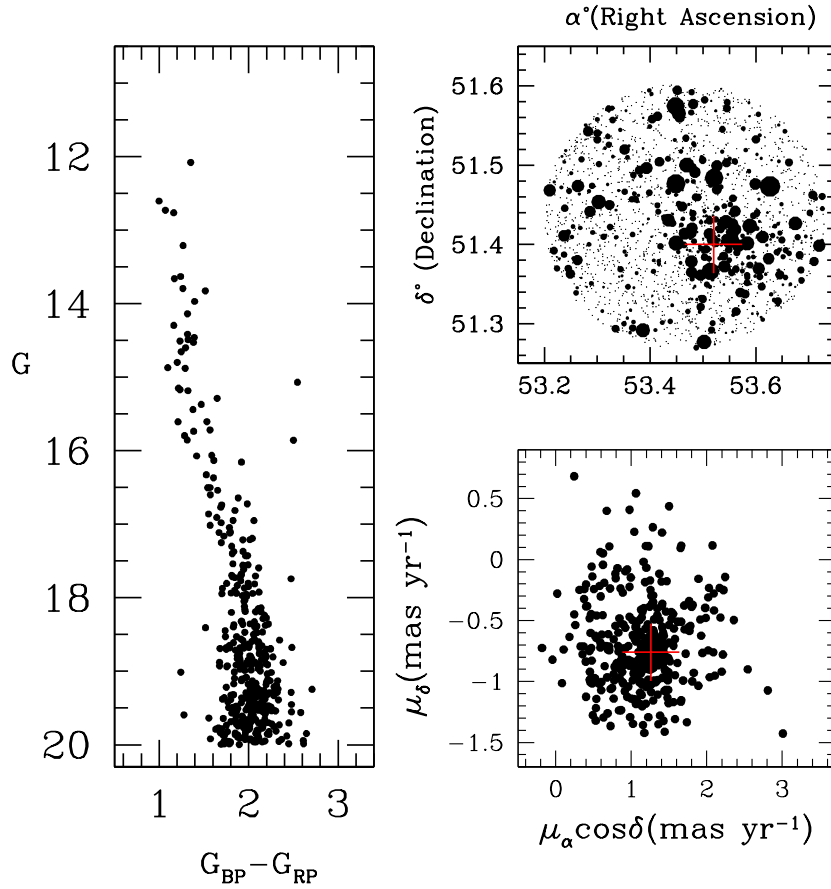


Fig. 6. ($G, G_{BP} - G_{RP}$) CMD, identification chart and proper motion distribution of member stars with membership probability higher than 50%. The plus sign indicates the cluster center.

4 Clusters Structure, extinction law and fundamental parameters evaluation

4.1 Cluster radius and radial stellar surface density

To estimate the cluster's center, the weighted mean of the positions of all stars has been considered by von Hoerner (1960, 1963). The center can be estimated by fitting a Gaussian function to the star's distribution and taking the center to be the point of maximum number density. We adopted this method to find the central coordinates of NGC 1348. This method has been described by Bisht et al. (2020). The central coordinates are found as $\alpha = 53.51 \pm 0.03$ deg ($3^h 34^m 2.3^s$) and $\delta = 51.41 \pm 0.02$ deg ($51^\circ 24' 36''$) which are in good agreement with the values given in Dias et al. (2002).

After center estimation, the next step is to construct a radial density profile (RDP), for which, we have drawn many concentric rings around the cluster center using the above estimated values of center coordinates. We determined the stellar number density, ρ_i , in the i^{th} zone of the cluster by using the relation: $\rho_i = \frac{N_i}{A_i}$, where N_i is the number of cluster members in the area A_i of the i^{th} zone. By fitting the King (1962) profile in this distribution as shown by a smooth continuous line in Fig. 7, we determined the structural properties of the cluster. The King (1962) profile is given as:

$$f(r) = f_{bg} + \frac{f_0}{1+(r/r_c)^2}$$

where r_c , f_0 , and f_{bg} are the core radius, central density, and the background density level, respectively.

We have shown background density level with errors using dotted lines in Fig. 7. At $r \sim 7.5'$ cluster stars get merged with the non-member stars, as shown clearly in Fig. 7. Hence, we considered $7.5'$ as the cluster radius. The error bars are calculated using the Poisson statistics error in each shell as $P_{err} = \frac{1}{\sqrt{N}}$. By fitting the King model to the cluster density profile, the structural parameters are found as: $f_b=2.54$ star/arcmin², $f_0=10.15$ star/arcmin² and $r_c=3.2$ arcmin. We obtained the density contrast parameter (δ_c) using the formula described by Bisht et al. (2020), which indicates that NGC 1348 is a sparse cluster. The tidal radius of clusters is normally influenced by the effects of Galactic tidal fields and later by internal relaxation dynamical evolution of clusters (Allen & Martos 1988). To calculate the tidal radius of NGC 1348, we used the formula derived by Bertin & Varri (2008) as:

$$r_t = \left(\frac{GM_{cl}}{\omega^2 \nu} \right)^{1/3}$$

where ω and ν are

$$\omega = (d\Phi_G(R)/dR)_{R_{gc}}/R_{gc})^{1/2}$$

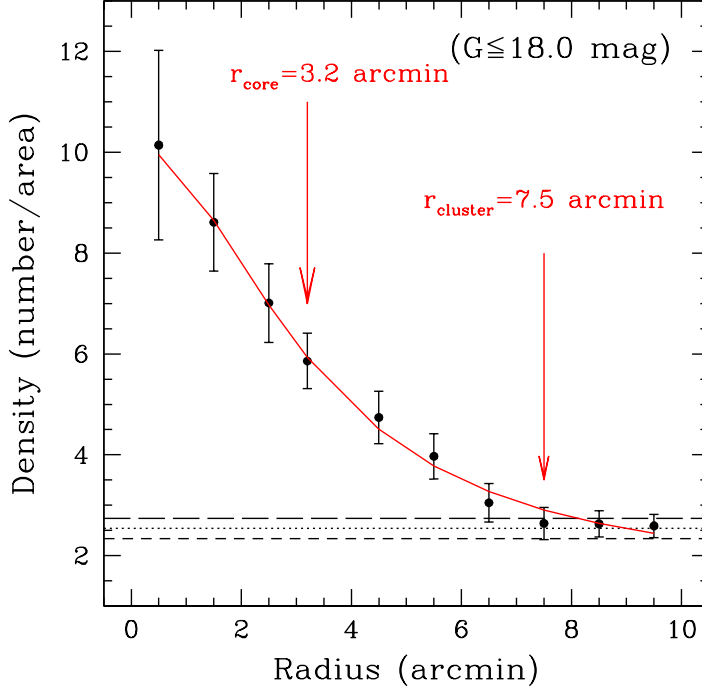


Fig. 7. Surface density distribution of the cluster NGC 1348 using GAIA EDR3 G band data. Errors are determined from sampling statistics ($=\frac{1}{\sqrt{N}}$ where N is the number of cluster members used in the density estimation at that point). The smooth line represents the fitted profile of King (1962) whereas the dotted line shows the background density level. Long and short dash lines represent the errors in background density.

$$\nu = 4 - \kappa^2/\omega^2$$

where κ is

$$\kappa = (3\omega^2 + (d^2\Phi_G(R)/dR^2)_{R_{gc}})^{1/2}$$

here Φ_G is Galactic potential, M_{cl} mass of the cluster, R_{gc} is the Galactocentric distance of the cluster, ω is the orbital frequency, κ is epicyclic frequency and ν is a positive constant. We used the Galactic potentials discussed in section 5. The value of the Galactocentric distance is taken from Table 1 and mass of the cluster is taken from section 6. In this manner, the tidal radius of the cluster is calculated as 9.2 pc.

4.2 Optical to mid-infrared extinction law

We have matched the multi-wavelength photometric data with Gaia astrometry to study the extinction law in various wavebands for NGC 1348. We plotted various $(\lambda - G_{RP})/(G_{BP} - G_{RP})$ two-color

Table 1. Multi-band color excess ratios in the direction of NGC 1348.

Band (λ)	Effective wavelength	$\frac{\lambda - G_{RP}}{G_{BP} - G_{RP}}$
Johnson B	445	1.66 ± 0.01
Johnson V	551	1.05 ± 0.02
Pan-STARRS g	481	1.42 ± 0.02
Pan-STARRS r	617	0.73 ± 0.03
Pan-STARRS i	752	0.15 ± 0.03
Pan-STARRS z	866	-0.16 ± 0.05
Pan-STARRS y	962	-0.35 ± 0.04
UKIDSS J	1234.5	-0.79 ± 0.03
UKIDSS H	1639.3	-1.21 ± 0.03
UKIDSS K	2175.7	-1.35 ± 0.06
WISE W1	3317.2	-1.39 ± 0.06
WISE W2	4550.1	-1.40 ± 0.07

diagrams (TCDs) as shown in Fig. 8. Here, λ represent the filters other than G_{RP} . A linear fit was executed in all TCDs to find the slope, which are listed in Table 1. These values of slopes are in fair agreement with the value described by Wang and Chen (2019). The value of total-to-selective absorption ratios $R_{cluster}$ in the range of ~ 2.9 -3.3 for different pass bands demonstrates that the reddening law is normal towards the cluster region of NGC 1348.

4.3 Reddening from UKIDSS colors

The $(J - H)$ versus $(J - K)$ color-color diagram plot has been used to obtain the value of interstellar reddening as shown in Fig 9. The solid line represents the Zero age main sequence (ZAMS) as taken from Caldwell et al. (1993). The similar ZAMS shown by the dotted line is displaced by $E(J - H) = 0.27 \pm 0.03$ mag and $E(J - K) = 0.47 \pm 0.05$ mag. The color excess ratio ($\frac{E(J-H)}{E(J-K)}=0.57$) is showing agreement with the normal value of 0.55 given by Cardelli et al. (1989). We obtained the value of interstellar reddening ($E(B - V)$) as 0.88 mag. Our estimated value is in good agreement with Carraro (2002). Our criterion for reddening estimation is admissible in exceptionally extended regions.

4.4 Age, distance and Galactocentric coordinates

The main fundamental parameters (age, distance, and reddening) have been obtained by fitting the theoretical isochrones of Marigo et al. (2017) to all the CMDs as shown in Fig. 10. The observed data

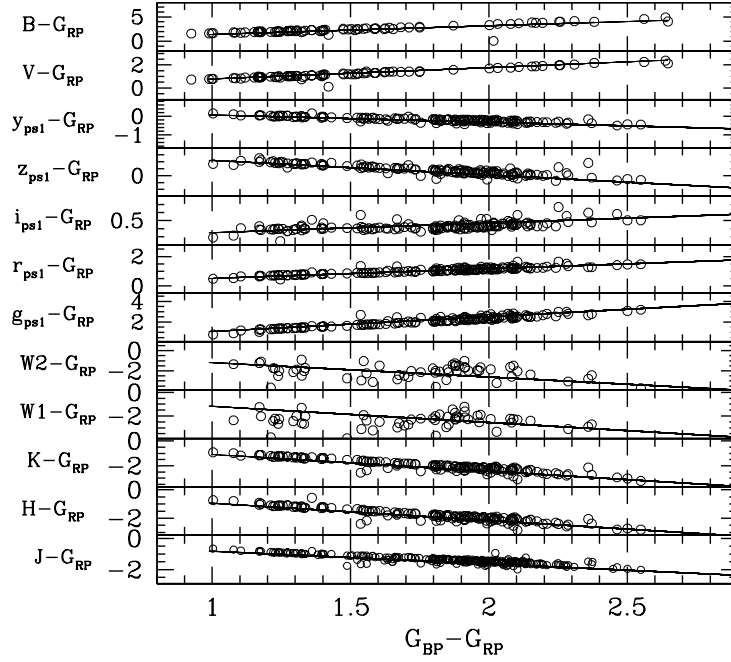


Fig. 8. The $(\lambda - G_{RP})/(G_{BP} - G_{RP})$ TCDs for the stars selected from VPD of NGC 1348. The continuous blue lines represent the slope determined through the least-squares linear fit.

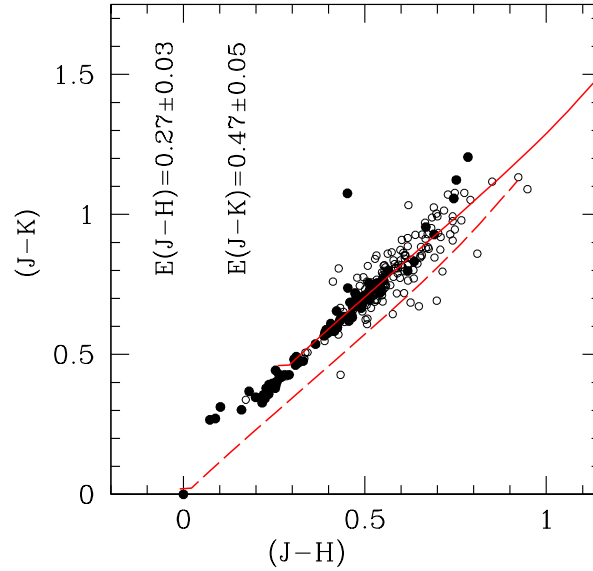


Fig. 9. The color-color diagram (CCD) for NGC 1348 using the probable cluster members. In this figure, the red solid line is the ZAMS taken from Caldwell et al. (1993) while the red dotted line is the same ZAMS shifted by the values given in the text. Solid black dots are the stars matched with Cantat-Gaudin et al. (2018).

have been corrected for reddening using the coefficients ratios $\frac{A_J}{A_V}=0.276$ and $\frac{A_H}{A_V}=0.176$, which are taken from Schlegel et al. (1998), while the ratio $\frac{A_{K_s}}{A_V}=0.118$ was derived from Dutra et al. (2002). For the Gaia DR2, we have estimated the mean value of A_G and $E(G_{BP} - G_{RP})$ as 1.92 and 0.96 using stars with membership probability higher than 50%. Cantat-Gaudin et al. (2018) catalog contains the membership probabilities of many OCs. In this paper, we have matched our likely members with their catalog and selected common stars having probability higher than 50%. These matched stars have been plotted in the CMDs as shown in Fig. 10.

The isochrones of different ages ($\log(\text{age})=8.10, 8.20$ and 8.30) with $Z = 0.008$ have been over plotted on all the CMDs for the cluster NGC 1348 as shown in Fig 10. The overall fit is satisfactory for $\log(\text{age})=8.20$ (middle isochrone) to the brighter stars, corresponding to 160 ± 40 Myr. The estimated distance modulus ($(m - M)=13.80$ mag) provides a distance from the Sun that is 2.4 ± 0.10 kpc.

4.4.1 Distance of the cluster using parallax angle

The distance can be estimated using the mean parallax of probable member stars (Luri et al. 2018). By using weighted mean method, the mean parallax for the cluster is found to be 0.39 ± 0.005 mas. Bailer-jones (2015) have shown that the distance estimation just by inverting the parallax is not reliable when there is an associated error. They described that a correct approach is to obtain the distance values from the parallaxes of stars through probabilistic analysis which includes a combination of a likelihood (measurements) and prior (assumption). Bailer-jones (2015) investigated different types of priors and Bailer-Jones (2018) suggested a exponentially decreasing space density prior in distance r . The prior depends upon a length scale parameter which can be obtained by fitting a three dimensional model of the Galaxy observed by Gaia and varies smoothly as a function of Galactic longitude and latitude. With the help of this prior, distance of the object can be calculated using a posterior which is similar as the likelihood (a Gaussian distribution function in parallax) but a function of distance. This method gives a pure geometric distance of objects which is independent of physical properties of interstellar extinction towards an individual star. Before calculating the distance we corrected the parallax for the offset (-0.017 mas) as suggested by Lindegren et al. (2020) for Gaia EDR3 data set. Then by adopting the above mentioned method the distance is estimated as 2.6 ± 0.05 kpc. This value of the cluster's distance is in good agreement with our result obtained from the isochrone fitting method.

5 Orbits of NGC 1348

Galactic orbits are very useful to explain the dynamical characteristics of clusters. We derive orbits and orbital parameters of NGC 1348 using Galactic potential models discussed by Allen & Santillan

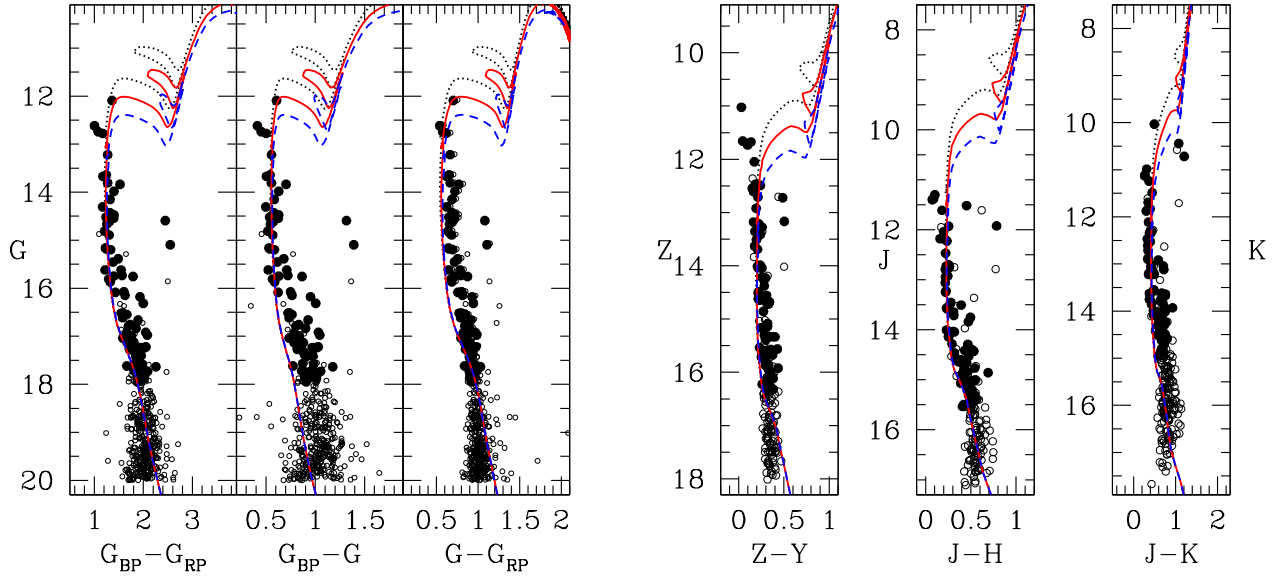


Fig. 10. The G , $(G_{BP} - G_{RP})$, G , $(G_{BP} - G)$, G , $(G - G_{RP})$, Z , $(Z - Y)$, J , $(J - H)$ and K , $(J - K)$ color-magnitude diagrams of open star cluster NGC 1348. These stars are probable cluster members. The curves are the isochrones of $(\log(\text{age})=8.10, 8.20 \text{ and } 8.30)$. These isochrones are taken from Marigo et al. (2017). Solid black dots are matched stars with Cantat-Gaudin et al. (2018).

(1991). Bajkova & Bobylev (2016) and Bobylev et al. (2017) refined the Galactic potential model parameters with the using new observational data for a distance $R \sim 0\text{--}200$ kpc. The description of these Galactic potential models is given by Rangwal et al. (2019).

The input parameters required to calculate orbits of the cluster, such as central coordinates (α and δ), mean proper motions ($\mu_{\alpha} \cos \delta$, μ_{δ}), parallax angles, age and heliocentric distance (d_{\odot}) have been taken from our investigation in this paper. The radial velocity for this object is not available in the literature. Average radial velocity for NGC 1348 was calculated by taking the mean of 14 probable cluster members as selected from the Gaia DR2 catalog. After five iterations, the average radial velocity is found as -18.71 ± 1.60 km/sec.

The right-handed coordinate system is used to convert equatorial velocity components into Galactic-space velocity components (U, V, W), where U , V and W are radial, tangential and vertical velocities respectively. Here, the x-axis is taken positive towards the Galactic-center, the y-axis is along the direction of Galactic rotation and the z-axis is towards the Galactic north pole. Galactic center is taken at $(17^h 45^m 32^s.224, -28^{\circ} 56' 10'')$ and the North-Galactic pole is taken to be located at $(12^h 51^m 26^s.282, 27^{\circ} 7' 42''.01)$ (Reid & Brunthaler, 2004). To apply a correction for Standard Solar Motion and Motion of the Local Standard of Rest (LSR), we used position coordinates of the Sun as $(8.3, 0, 0.02)$ kpc and its space-velocity components as $(11.1, 12.24, 7.25)$ km/s (Schönrich et al.

Table 2. Position and velocity components in Galactocentric coordinate system. Here R is the Galactocentric distance, Z is vertical distance from the Galactic disc, U V W are radial tangential and vertical components of velocity respectively, and ϕ is the position angle relative to the sun's direction.

Cluster	R	Z	U	V	W	ϕ
	(kpc)	(kpc)	(km/sec)	(km/sec)	(km/sec)	(radians)
NGC 1348	10.39	-0.14	-11.71 ± 1.68	-232.55 ± 1.51	-10.14 ± 1.65	0.13

Table 3. The obtained orbital parameters using Galactic potential model.

Cluster	e	R_a	R_p	Z_{max}	Birth position	E	J_z	T
		(kpc)	(kpc)	(kpc)	(R,Z)	$(100km/sec)^2$	(100 kpc km/s)	(Myr)
NGC 1348	0.004	10.47	10.38	0.25	(11.47,0.30)	-9.88	-24.38	284

2010). The transformed parameters in the Galactocentric coordinate system are listed in Table 2.

Fig. 11 shows orbits of the cluster NGC 1348. In the top left panel, the motion of the cluster is described in terms of distance from Galactic center and Galactic plane, which indicates the 2D side view of the orbit. In the top right panel, the cluster motion projected into the plane of the Galaxy is described, which shows the top view of orbit. The bottom panel of this figure indicates the distance of NGC 1348 from the Galactic plane as a function of time. The nearly circular orbit of NGC 1348 follows a boxy pattern. However the cluster shows a small drift of ~ 83 pc from the circular motion. The birth and the present day position of NGC 1348 in the Galaxy are represented by filled triangle and circle in Fig. 11. We also calculated the orbital parameters for the clusters which are listed in Table 3. Here e is eccentricity, R_a is apogalactic distance, R_p is perigalactic distance, Z_{max} is the maximum distance traveled by cluster from Galactic disc, E is the average energy of orbits, J_z is z component of angular momentum and T is time period of the revolution around the Galactic center. The orbital parameters determined in the present analysis are similar to the parameters determined by Wu et al. (2009).

6 Dynamics of the cluster

6.1 Luminosity and mass function

Distribution of the cluster members in a unit magnitude range is called the luminosity function (LF). To derive the LF, we used only the probable members of NGC 1348. To construct the LF, we converted

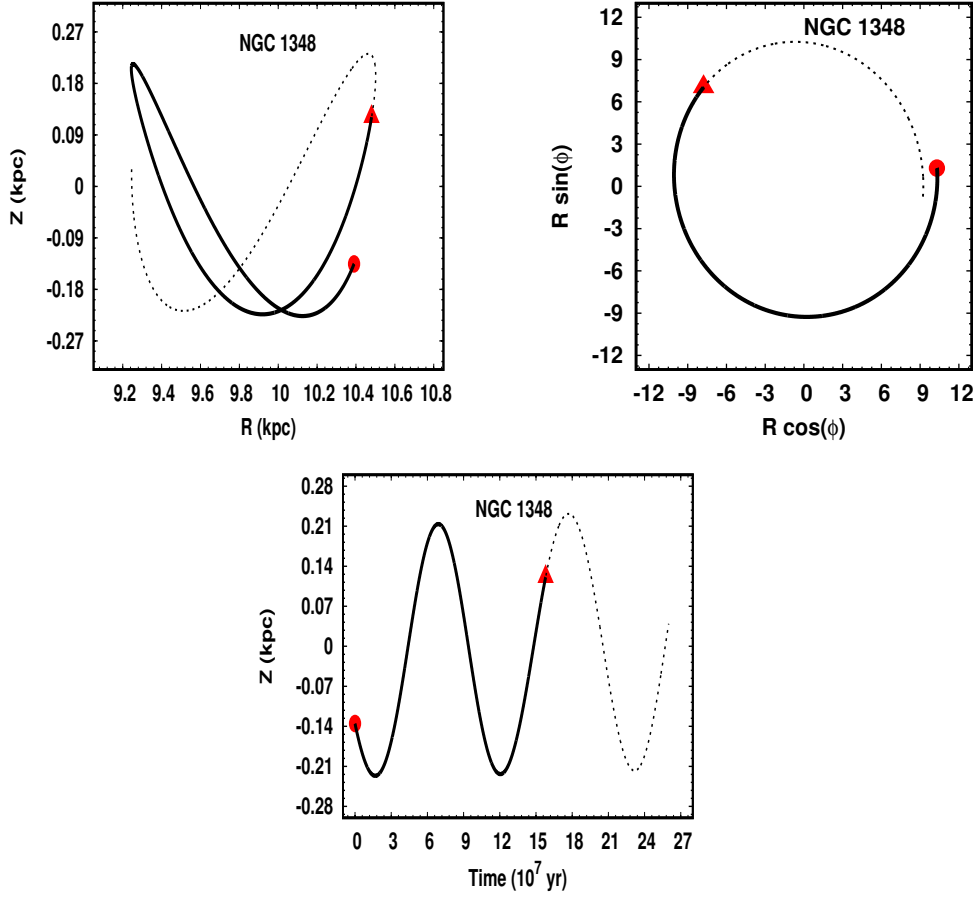


Fig. 11. Galactic orbits of the cluster NGC 1348 estimated with the Galactic potential model described in the text in the time interval equal to the age of the cluster. The top left panel shows the side view and the top right panel shows the top view of the orbit. Bottom panel shows the distance of cluster from the Galactic plane as a function of time. Dotted line represents the cluster's orbits for a time interval of 284 Myr. The filled circle and the triangle sign denote the birth and the present day position of cluster in the Galaxy.

the apparent G magnitudes into the absolute ones using the distance modulus. The resulting histogram is shown in the left panel of Fig. 12. This figure shows that the LF continues rising up to $M_G \sim 2.9$ mag.

The LF and mass function (MF) are associated with each other according to the mass-luminosity relation (MLR). We have used the theoretical tables of evolutionary tracks of Marigo et al. (2017) to convert luminosities into masses. Fig. 12 displays the luminosity function of member stars of the cluster (left panel) and the derived present day mass function (PDMF; right panel). The PDMF, under specific conditions is an approximate representation of the IMF.

The shape of the present day mass function of stars in NGC 1384 for masses $\geq 1 M_{sol}$ can be approximated by a power law of the form,

$$\log \frac{dN}{dM} = -(1+x) \log(M) + \text{constant} \quad (1)$$

Where dN is the number of stars in the mass interval $M+dM$. We derive a value of $x = 1.30 \pm 0.18$, which is close to the value of 1.35 derived by Salpeter (1955) for the nearby Galactic field. It is worth mentioning that the slope of the mass function of the Galactic field is being constantly updated using more modern data and sophisticated inference techniques. A recent work by Mor et al. (2019) inferred a shallower than Salpeter slope for the Galactic IMF (close to -1) which is in agreement with the theoretical prediction of Dib & Basu (2018). Dib et al. (2017) inferred the distribution function of the slope of the IMF for a large population of Galactic clusters and found that it is well represented by a Gaussian distribution centered around the Salpeter value but with a standard deviation of 0.6. For NGC 1348, our derived value falls well within this range, when considering the uncertainty we have measured for the slope. The total mass was obtained as $\sim 215 M_{sol}$.

6.2 Mass-segregation study

The mass segregation effect in the clusters has been described by many authors (e.g. Sagar et al. 1988; Hillenbrand & Hartmann 1998; Fisher et al. 1998; Meylan 2000; Baumgardt & Makino 2003; Dib, Schmeja & Parker 2018; Dib & Henning 2019; Alcock & Parker 2019). To understand this effect in NGC 1348, we divided the mass range in two subranges as $1.5 \leq \frac{M}{M_{\odot}} \leq 4.1$ and $1 \leq \frac{M}{M_{\odot}} \leq 1.5$. The cumulative radial stellar distribution of stars for two different mass ranges as shown in Fig. 13. This figure demonstrates the mass-segregation effect as bright stars appear to be more centrally concentrated than the low mass members. This has been checked through Kolmogorov-Smirnov test ($K-S$). In this way, we found that the confidence label of the mass-segregation effect is 91 %.

The possible reason of the mass-segregation effect generally differs from one cluster to another. This may be because of dynamical evolution or could be an imprint of star formation or both (Dib, Kim & Shadmehri 2007; Allison et al. 2009; Pavlik 2020). The most important result of this process is that the most massive stars sink gradually towards the cluster center and transfer their kinetic energy to the more numerous lower-mass stars, thus leading to mass segregation. The relaxation time T_E is defined as the time in which the stellar velocity distribution becomes Maxwellian and expressed by the following formula:

$$T_{ES} = \frac{8.9 \times 10^5 \sqrt{N} \times R_h^{3/2}}{\sqrt{\bar{m}} \times \log(0.4N)} \quad (2)$$

where N represents the number of stars in the clusters (in our case the ones with membership probability higher than 50%), R_h is the cluster half mass radius expressed in parsec and \bar{m} is the

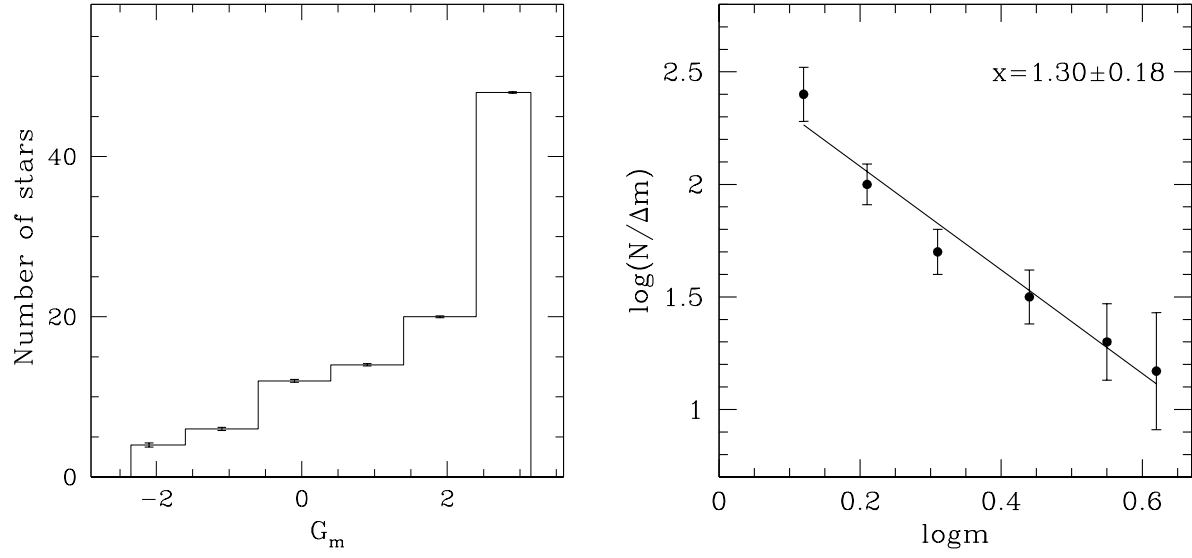


Fig. 12. (Left panel) Luminosity function of stars in the region of the cluster NGC 1348. (Right panel) Mass function derived using the most probable members, where solid line indicates the power law given by Salpeter (1955). The error bars represent $\frac{1}{\sqrt{N}}$.

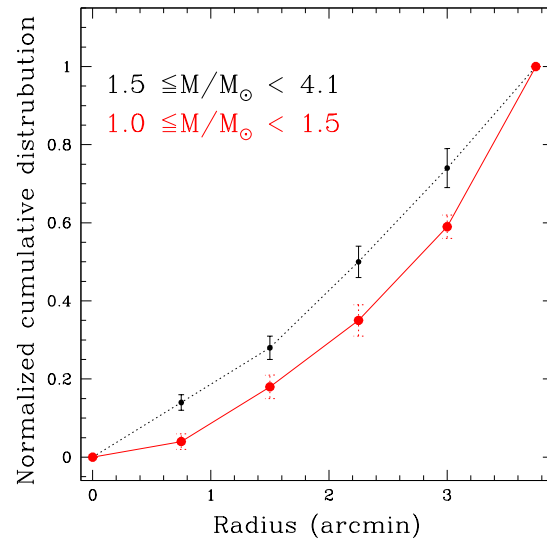


Fig. 13. The cumulative radial distribution for NGC 1348 using the most probable members in several mass ranges.

average mass of the cluster members (Spitzer & Hart 1971) in the solar unit. The value of \bar{m} is found as $2.07 M_{\odot}$. The value of R_h is assumed to be equal to half of the cluster's extent. Using the above formula, the value of dynamical relaxation time T_{ES} is determined as 18 Myr¹. Hence, we conclude that NGC 1348 is a dynamically relaxed cluster.

7 Kinematical structure of NGC 1348

• *Vertex (apex position) of the cluster*

The Apex coordinates are obtained by solving the geometric problems in which the intersection of vectors of spatial velocities (i.e. V_x, V_y, V_z) of stars on the celestial sphere, when the beginning of the vectors is moved to the point of observations. A formal description of the method, diagramming technique, and formulas to determine the error ellipses can be found in Chupina et al. (2001, 2006). This method has been used previously by some of us (Vereshchagin et al. 2014, Elsanhoury et al. 2018, Elsanhoury 2020a, 2020b, Postnikova et al. 2020). The equatorial coordinates of the convergent point have the following forms:

i.e.

$$A_o = \tan^{-1} \left[\frac{\overline{V_y}}{\overline{V_x}} \right]. \quad (3)$$

$$D_o = \tan^{-1} \left[\frac{\overline{V_z}}{\sqrt{\overline{V_x}^2 + \overline{V_y}^2}} \right]. \quad (4)$$

The apex equatorial coordinates for NGC 1348 are presented here with Fig. 14.

We have also derived several kinematical parameters, for example, the matrix elements (μ_{ij}), direction cosines (l_j, m_j, n_j) etc. using techniques described by Bisht et al. (2020). All these parameters are listed in Table 4.

8 Conclusions

We conducted an exhaustive photometric and kinematical study of the poorly studied northern open cluster NGC 1348 using UKIDSS, WISE, APASS, Pan-STARRS1 and Gaia EDR3 data sets. We calculated the membership probabilities of the stars in NGC 1348 and hence found 438 member stars with membership probabilities higher than 50% and $G \leq 20$ mag. To derive the fundamental parameters of the cluster, we used only these selected member stars. We also shed some light on the dynamical and kinematical properties of the cluster. Our main findings are summarized follows:

¹ This value is obtained using stars with mass $\geq 1 M_{\odot}$. If we include the low mass stars ($\geq 0.1 M_{\odot}$), the value of the relaxation time becomes ~ 52 Myr. In either case, the cluster is dynamically relaxed according to this study.

Table 4. Dynamical and kinematical parameters of NGC 1348.

Parameters	Numerical values	Reference
No. of members (N)	438	Present study
Age (log)	8.20	Present study
(A_o, D_o)	$-23.815 \pm 0.135, -22.228 \pm 0.105$	Present study
Cluster radius (arcmin)	7.5	Present study
Cluster radius (pc)	5.67	Present study
$T_{ES}(\text{Myr})$	18.00	Present study
τ	8.886 ± 0.413	Present study
$(\overline{V_x}, \overline{V_y}, \overline{V_z}), (\text{km s}^{-1})$	$94.40 \pm 0.10, -41.63 \pm 0.15, -42.13 \pm 0.15$	Present study
$(\overline{V_\alpha}, \overline{V_\delta}, \overline{V_t}), (\text{km s}^{-1})$	$-100.57 \pm 0.10, -43.95 \pm 0.15, 153.78 \pm 0.09$	Present study
$(\lambda_1, \lambda_2, \lambda_3) (\text{km s}^{-1})$	5765040, 19837.3, 348.674	Present study
$(\sigma_1, \sigma_2, \sigma_3) (\text{km s}^{-1})$	2401.05, 140.845, 18.673	Present study
$(l_1, m_1, n_1)^\circ$	0.339, 0.404, -0.850	Present study
$(l_2, m_2, n_2)^\circ$	$-0.431, -0.737, -0.522$	Present study
$(l_3, m_3, n_3)^\circ$	0.837, $-0.543, 0.076$	Present study
$(x_c, y_c, z_c) (\text{kpc})$	$-8.811, -11.911, -18.486$	Present study
$B_j, j=1, 2, 3$	$-58^\circ.197, -31^\circ.436, 4^\circ.340$	Present study
$L_j, j=1, 2, 3$	$-50^\circ.030, 120^\circ.283, -147^\circ.059$	Present study
$X_\odot (\text{kpc})$	-2.175 ± 0.047	Present study
	-1.933	Cantat-Gaudin <i>et al.</i> (2020)
$Y_\odot (\text{kpc})$	1.414 ± 0.038	Present study
	1.2568	Cantat-Gaudin <i>et al.</i> (2020)
$Z_\odot (\text{kpc})$	-0.168 ± 0.013	Present study
	-0.1495	Cantat-Gaudin <i>et al.</i> (2020)
$R_{gc} (\text{kpc})$	10.476 ± 0.102	Present study
	10.349	Cantat-Gaudin <i>et al.</i> (2020)
$S_\odot (\text{km/s})$	111.36	Present study
$(l_A, \alpha_A)_{w.s.v.c.}$	$-32.21, 56.58$	Present study
$(b_A, \delta_A)_{w.s.v.c.}$	$-23.82, 22.23$	Present study

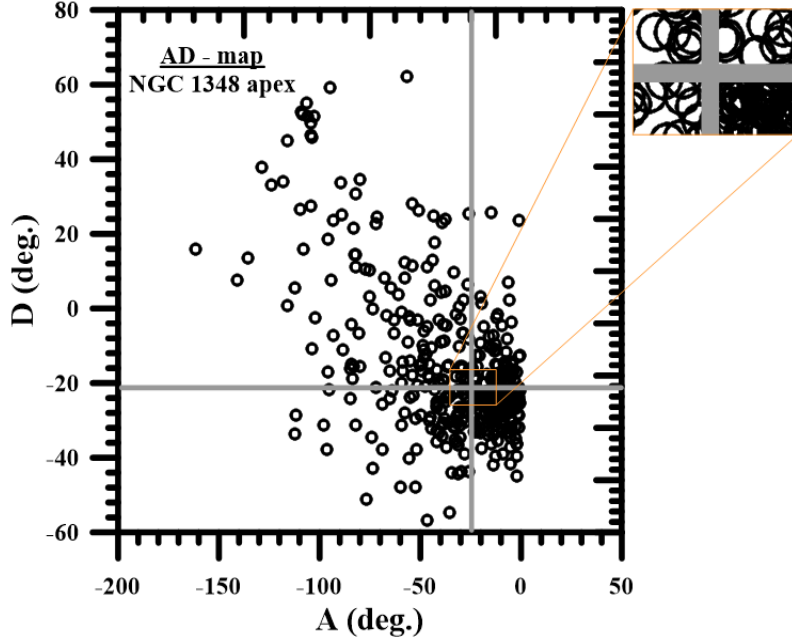


Fig. 14. The convergent point of NGC 1348 open cluster with AD-chart method, showing the apex coordinates

$$(A_o, D_o) = (13.865 \pm 0.238, -48.348 \pm 0.144).$$

- The cluster's center is obtained as: $\alpha = 53.51 \pm 0.03$ deg ($3^h 34^m 2.3^s$) and $\delta = 51.41 \pm 0.02$ deg ($51^\circ 24' 36''$) with the help of the most probable cluster members. The radius of the cluster is determined as 7.5 arcmin using a radial density profile.
- Based on the vector point diagram and membership probability estimation of stars, we identified 438 most probable cluster members for this object. The mean PMs of the cluster is estimated as 1.27 ± 0.001 and -0.73 ± 0.002 mas yr $^{-1}$ in both the RA and DEC directions respectively.
- The distance is determined as 2.6 ± 0.05 kpc. This value is in fair agreement with the distance estimated using the mean parallax of the cluster. Age is determined as 160 ± 40 Myr by comparing the cluster's CMD with the theoretical isochrones given by Marigo et al. (2017).
- The mass function slope is estimated as 1.30 ± 0.18 , which is in good agreement with the value (1.35) given by Salpeter (1955) for field stars in Solar neighborhood.
- Mass segregation is also observed for NGC 1348. The K-S test indicates 91% confidence level of the mass-segregation effect. Our study indicates that NGC 1348 is a dynamically relaxed open cluster.
- The Galactic orbits and orbital parameters were estimated using Galactic potential models. We found that NGC 1348 is orbiting in a boxy pattern.
- The apex position (A, D) is computed with the AD-chart methods as: $(A_o, D_o) = (-23^\circ.815 \pm 0^\circ.135, -22^\circ.228 \pm 0^\circ.105)$ respectively.
- We computed the direction cosines (l_j, m_j, n_j) in three axes.

- The projected distance ($X_{\odot}, Y_{\odot}, Z_{\odot}$ are computed as $(-2.175 \pm 0.047, 1.414 \pm 0.038, -0.168 \pm 0.013)$ kpc and the Solar elements (S_{\odot}, l_A, b_A) are derived as $(111.36, -32^{\circ}.21, 56^{\circ}.58)$.

ACKNOWLEDGMENTS

The authors thank the anonymous referee for the useful comments that improved the scientific content of the article significantly. This work has been financially supported by the Natural Science Foundation of China (NSFC-11590782, NSFC-11421303). Devesh P. Sariya and Ing-Guey Jiang are supported by the grant from the Ministry of Science and Technology (MOST), Taiwan. The grant numbers are MOST 105-2119-M-007 -029 -MY3 and MOST 106-2112-M-007 -006 -MY3. This work has made use of data from the European Space Agency (ESA) mission GAIA processed by Gaia Data processing and Analysis Consortium (DPAC), (<https://www.cosmos.esa.int/web/gaia/dpac/consortium>).

References

- Alcock, H. & Parker R. J. 2019, MNRAS, 490, 350A
- Allen, C. & Martos, M. 1988, RMxAA, 16, 25
- Allen, C. & Santillan, A. 1991, Rev. Mexicana Astron. Astrofis., 22, 255
- Allison R. J., Goodwin S. P., Parker R. J., de Grijs R., Zwart S. F. P., Kouwenhoven M. B. N., 2009, The Astrophysical Journal, 700, L99
- Arenou, F., Luri, X., Babusiaux, C. et al. 2018, A&A, 616, A17
- Bailer-Jones C. A. L., 2015, PASP, 127, 994
- Bailer-Jones C. A. L., Rybizki J., Fouvresneau M., Mantelet G., Andrae R., 2018, AJ, 156, 58
- Bajkova, A. T. & Bobylev, V. V. 2016, Astronomy Letters, 42, 9
- Baumgardt, H. & Makino, J., 2003, MNRAS, 340, 227
- Bertin G., Varri A. L., 2008, ApJ, 689, 1005
- Bisht, D., Yadav, R. K. S. & Durgapal, A. K. 2017, NewA, 52, 55B
- Bisht, D., Yadav, R. K. S., Ganesh, S., Durgapal, A. K., Rangwal, G. & Fynbo, J. P. U. 2019, MNRAS, 482, 1471B
- Bisht, D., Elsanhoury W., Zhu, Q., Sariya, D. P. et al., 2020, AJ, 160, 119
- Bisht, Zhu, Q., Yadav, R. K. S. et al., 2021a, AJ, 161, 182
- Bisht, Zhu, Q., Yadav, R. K. S. et al., 2021b, Accepted (arXiv:2103.04596)
- Bland-Hawthorn J., Sharma S. et al., 2019, MNRAS, 486, 1167.

Brown A., 1950, ApJ, 112, 225

Bobylev, V. V., Bajkova, A. T. & Gromov, A. O. 2017, Astronomy Letters, 43, 4

Cantat-Gaudin, T., Jordi, C., Vallenari, A., et al. 2018, A&A, 618A, 93C

Cantat-Gaudin & Anders, F. 2020, A&A, 633A, 99C

Caldwell, J. A. R., Cousins, A. W. J., Ahlers, C. C., van Wamelen, P. & Maritz, E. J. 1993, South Astronomical Observatory, Circ No. 15

Cardelli, J. A., Clayton, G. C. & Mathis, J. S. 1989, ApJ, 345, 245

Carraro, G., Ng, Y. K., & Portinari, L. 1998, MNRAS, 296, 1045

Carraro, G., 2002, A&A, 387, 479C

Casali, M. et al. 2007, A&A, 467, 777

Castro-Ginard A., et al. 2020, A&A, 635, A45

Chen, L., Hou, J. L., & Wang, J. J. 2003, AJ, 125, 1397

Chupina, N. V., Reva, V. G., Vereshchagin, S. V., 2001. A&A, 371, 115.

Chupina, N. V., Reva, V. G., Vereshchagin, S. V., 2006. A&A, 451, 909.

de Bruijne J. H. J., 1999, MNRAS, 306, 381

Dias, W. S., Alessi, B. S., Moitinho, A., Lepine, J. R. D., 2002, A&A, 389, 871

Dib, S. & Basu, S. 2018, A&A, 614, A43

Dib, S. & Henning, T. 2019, A&A, 629, 135

Dib, S., Kim, J., & Shadmehri, M. 2007, MNRAS, 381, L40

Dib, S. 2014, MNRAS, 444, 1957

Dib, S., Schmeja, S., & Hony, S. 2017, MNRAS, 464, 1738

Dib, S., Schmeja, S., & Parker, R. J. 2018, MNRAS, 473, 849

Durgapal, A. K. & Pandey, A. K. 2001, A&A, 375, 840

Dutra, C., Santiago, B. & Bica, E. 2002, A&A, 381, 219

Eggen O. J. 1984, Astron. J., 89, 1350

Elmegreen, B. G. 2000, ApJ, 539, 342

Elsanhoury, W. H. et al. 2015, Rev. Mex. Astron. Astrofis, 51, 197

Elsanhoury, W. H. et al. 2018. Astrophysics and space science, 363, 58.

Elsanhoury, W. H. et al. 2020a, Astronomy reports, 64, 94

Elsanhoury, W. H. et al. 2020b, Astronomy reports, 64, 199

Fischer P., Pryor C., Murray S., Mateo M., Richtler T., 1998, AJ, 115, 592

Gaia Collaboration, Brown, A. G. A., et al. 2020, arXiv:2012.01533 Gaia Collaboration et al. 2018a, A&A, 616, A1

Gaia Collaboration et al. 2018b, A&A, 616, A11

Galli P. A. B., Teixeira R., Ducourant C., Bertout C. & Benevides-Soares P. 2012, *Astron. Astrophysics*, 538, 23

Gunn J. E., Griffin R. F., Griffin R. F. M. & Zimmerman B. A. 1998, *Astron. J.*, 97, 198

Hanson, R. B. 1975, *Astron. J.*, 80, 379

Henden, A., Munari, U. 2014, *Contrib. Astron. Obs. Skalnate Pleso*, 43, 518

Heden, A., Templeton, M., Terrell, D., et al. 2016, *VizieR Online Data Catalog*, II/336

Hewett P. C., Warren S. J., Leggett S. K., Hodgkin S. T., 2006, *MNRAS*, 367, 454

Hillenbrand L. A., Hartmann L. W., *ApJ*, 492, 540

Hodapp, K. W., Kaiser, N., Aussel, H., et al. 2004, *AN*, 325, 636

Janes K.A., Adler D., 1982, *ApJS* 49, 425.

Jones D. H. P., 1971, *MNRAS*, 152, 231

King, I. 1962, *AJ*, 67, 471

Larson, R. B. 1999. Star formation. In: Nakamoto, T. (Ed.), *Nobeyama Radio Observatory*, Japan, p. 336

Luri X., et al., 2018, *A&A*, 616, A9

Lawrence A., et al. 2007, *MNRAS*, 379, 1599

Lindgren L., et al. 2020, *arXiv e-prints*, arXiv:2012.01742

Liu L., Pang X., 2019, *ApJS*, 245, 32

Marks, M., Kroupa, Pavel., Dabringhausen, Jorg., Pawlowski, Marcel S. 2012, *MNRAS*, 422, 2246M

Marigo, P. et al. 2017, *ApJ*, 835, 77

Meylan, G., 2000, Massive stellar clusters, conference held in strasbourg, france. In: Lanon, A., Boily, C. (Eds.), *Astronomical Society of the Pacific Conference Series*, p.215

Mihalas, D., Binney, J., 1981, *Galactic astronomy: structure and kinematics*/2nd edition.

Morau, E. 2016, *EAS*, 80, 73M

Pavlik, Vaclav. 2020, *A&A*, 638, A155

Phelps, R. L. & Janes, K. A. 1993, *AJ*, 106, 1870

Piatti, A. E., Bica, E., Santos, Jr., J. F. C. & Clariá, J. J. 2002, *A&A*, 387, 108P

Piskunov, A. E., Belikov, A. N., Kharchenko, N. V. & Sagar, R. 2004, *MNRAS*, 349, 1449

Piskunov, A. E., Kharchenko, N. V., Roser, S., Schilbach, E., & Scholz, R. D. 2006, *A&A*, 445, 545

Postnikova E. S., Elsanhoury W. H. et al., 2020, *RAA*, Vol. 20, No. 2, 16.

Rangwal, G., Yadav, R. K. S., Durgapal, A., Bisht, D. & Nardiello, D. 2019, *MNRAS*, 490, 1383

Reid M. J., Brunthaler A. 2004, *ApJ*, 616, 872

Sagar R., Myakutin V. I., Piskunov A. E., Dluhnevskaya O. B., 1988, *MNRAS*, 234, 831

Salpeter, E. E. 1955, *ApJ*, 121, 161

Sariya, D. P., Jiang, Ing-Guey., Sizova, M. D., et al. 2021a, *AJ*, 161, 101

Sariya, D. P., Jiang, Ing-Guey., Bisht, D., et al. 2021b, AJ, 161, 102

Schonrich, Ralph., Binney, James., Dehnen, Walter. 2010, MNRAS, 403, 1829S

Scalo, J. M. 1998, The stellar initial mass function. In: Gilmore, G., Parry, I., Ryan, S. (Eds.) ASP Conf, 142, p.201

Schlegel, D. J., Finkbeiner, D. P. & Davis, M. 1998, ApJ, 500, 525

Sim G., Lee S. H., Ann H. B., Kim S., 2019, JKAS, 52, 145

Smart W. M., 1938, Stellar Dynamics, Cambridge University Press.

Spitzer, L. & Hart, M. 1971, ApJ, 164, 399

Sung, H. & Bessell, M. S. 2004, AJ, 127, 1014

Tonry, J. L., Stubbs, C. W., Lykke, K. R., et al. 2012, ApJ, 750, 99

Tadross, A. L., 2011, JKAS, 44, 1T

Trumpler R.J., 1930, Lick Obs. Bull., 14, 154 (No. 420)

Vereshchagin, S. V., Chupina, N. V., Sariya, D. P., Yadav, R. K. S., & Kumar, B. 2014, New Astron., 31, 43.

von Hoerner, S. 1960, ZA, 50, 184V

von Hoerner, S. 1963, ZA, 57, 47

Wang S. & Chen X., 2019, ApJ, 877, 116W

Wayman, P. A., Symms, L. S. & Blackwell, K. C., 1965, R. Obs. Bull, 98

Wu, Z. Y., Zhou, X., Ma, J. & Du, C. H. 2009, MNRAS, 399, 2146

Yadav, R. K. S. & Sagar, R. 2002, MNRAS, 337, 133

Yadav, R. K. S. & Sagar, R. 2004, MNRAS, 349, 1481

Yadav R. K. S., Sariya D. P., Sagar R., 2013, MNRAS, 430, 3350

appendix

• *Galactic longitude of the vertex l_2*

Stars in the thick disk (~ 200 - 300 pc) of our Galaxy appear to have formed well after the formation of the spheroidal component of the Galaxy. As a result of nucleosynthesis in the stars, the distribution of velocity ellipsoids of the stars in the Galactic plane, will be expected to have one axis directed exactly towards the Galactic center; this is known as the longitude of the vertex (l_2 , Mihalas and Binney 1981). Our analysis of an ellipsoidal velocity distribution (Elsanhoury 2015 and 2020; Elsanhoury et al. 2016, 2018; & Bisht et al. 2020) confirmed that the longitude of the vertex often differs significantly from zero i.e. $l_2 = -0.728$ and gets affected by the stellar spectral classes (i.e. temperature scale).

• *The Galactic longitude and Galactic latitude parameters*

Let (L_i) and (B_i) , ($\forall j=1, 2, 3$) be the Galactic longitude and the Galactic latitude of the directions, respectively which correspond to the extreme values of the dispersion, then

$$L_j = \tan^{-1}\left(\frac{-m_j}{l_j}\right), \quad (5)$$

$$B_j = \sin^{-1}(n_j). \quad (6)$$

• *The center of the cluster*

The center of the cluster (x_c, y_c, z_c) can be derived by the simple method of finding the equatorial coordinates of the center of mass for the number (N_i) of discrete objects, i.e.

$$x_c = \left[\sum_{i=1}^N d_i \cos \alpha_i \cos \delta_i \right] / N, \quad (7)$$

$$y_c = \left[\sum_{i=1}^N d_i \sin \alpha_i \cos \delta_i \right] / N, \quad (8)$$

$$z_c = \left[\sum_{i=1}^N d_i \sin \delta_i \right] / N. \quad (9)$$

• *Projected distances*

Considering our estimated distances $d(\text{pc})$, we can calculate the distances to the Galactic center (R_{gc}) (Mihalas & Binney 1981) as a function of the Sun's distance from the Galactic center (i.e. $R_o = 8.20 \pm 0.10$ kpc) as mentioned recently with Bland-Hawthorn et al.(2019) as $R_{gc}^2 = R_o^2 + d^2 - 2R_o d \cos l$. The projected distances towards the Galactic plane (X_\odot, Y_\odot) and the distance from the Galactic plane (Z_\odot) (Tadross 2011) are computed as:

$$X_\odot = d \cos b \cos l, \quad (10)$$

$$Y_{\odot} = d \cos b \sin l, \quad (11)$$

$$Z_{\odot} = d \sin b. \quad (12)$$

• **Solar elements**

Let us consider a group with spatial velocities (\bar{U} , \bar{V} and \bar{W}). The components of the Sun's velocities (U_{\odot} , V_{\odot} , and W_{\odot}) are then given as: ($U_{\odot} = -\bar{U}$), ($V_{\odot} = -\bar{V}$), and ($W_{\odot} = -\bar{W}$). Therefore, we have the Solar elements With spatial velocities considered (w.s.v.c.) like;

$$S_{\odot} = \sqrt{\bar{U}^2 + \bar{V}^2 + \bar{W}^2}, \quad (13)$$

$$l_A = \tan^{-1} \left(\frac{-\bar{V}}{\bar{U}} \right), \quad (14)$$

$$b_A = \sin^{-1} \left(\frac{-\bar{W}}{S_{\odot}} \right). \quad (15)$$

Now, let us consider the positions along the x, y, and z-axes in the coordinate system which is centered at the Sun. Then, the Sun's velocities with respect to this same group and referred to the same axes are given as; ($X_{\odot}^{\bullet} = -\bar{V}_X$), ($Y_{\odot}^{\bullet} = -\bar{V}_Y$), and ($Z_{\odot}^{\bullet} = -\bar{V}_Z$). Therefore, we have obtained the Solar elements with radial velocities considered as;

$$S_{\odot} = \sqrt{(X_{\odot}^{\bullet})^2 + (Y_{\odot}^{\bullet})^2 + (Z_{\odot}^{\bullet})^2}, \quad (16)$$

$$\alpha_A = \tan^{-1} \left(\frac{Y_{\odot}^{\bullet}}{X_{\odot}^{\bullet}} \right), \quad (17)$$

$$\delta_A = \tan^{-1} \left(\frac{Z_{\odot}^{\bullet}}{\sqrt{(X_{\odot}^{\bullet})^2 + (Y_{\odot}^{\bullet})^2}} \right). \quad (18)$$

where (l_A , α_A) is the Galactic longitude and right ascension of the Solar apex and (b_A , δ_A) are the Galactic latitude and declination of the Solar apex. (S_{\odot}) is considered as the absolute value of the Sun's velocity relative to the stellar groups under investigation.